Journal of Scientific Computing (2019) 80:1913–1935
https://doi.org/10.1007/s10915-019-01006-0

A Conforming DG Method for Linear Nonlocal Models with Integrable Kernels

Qiang Du[1] · **Xiaobo Yin**[2]

Received: 6 February 2019 / Revised: 28 May 2019 / Accepted: 6 July 2019 / Published online: 11 July 2019

Abstract
The numerical solution of nonlocal constrained value problems with integrable kernels is considered. These nonlocal problems arise in nonlocal mechanics and nonlocal diffusion. The structure of the true solution to the problem is analyzed first. The analysis leads naturally to a new kind of discontinuous Galerkin method that can more efficiently solve the problem numerically. The new method is shown to be asymptotically compatible. Moreover, it has optimal convergence rate for any dimensional case under mild assumptions.

Keywords Nonlocal diffusion · Peridynamic model · Nonlocal model · Integrable kernel · Discontinuous Galerkin · Finite element · Convergence analysis · Condition number

Mathematics Subject Classification 82C21 · 65R20 · 74S05 · 46N20 · 45A05

1 Introduction

Nonlocal models have generated much interests in recent years [14]. For example, the peridynamic (PD) model proposed by Silling [26] is an integral-type nonlocal theory of continuum mechanics which provides an alternative setup to classical continuum mechanics based on PDEs. Since PD avoids the explicit use of spatial derivatives, it is especially effective for modeling problems involving discontinuities or other singularities in the deformation [6,19,22,24,28,29]. The nonlocal diffusion (ND) model, described in [16] is another example

This research is supported in part by National Science Foundation (DMS-1719699), Army Research Office (MURI W911NF-15-1-0562), National Natural Science Foundation of China (11671165, 91630201) and Program for Changjiang Scholars and Innovative Research Team in University IRT17R46.

✉ Xiaobo Yin
yinxb@mail.ccnu.edu.cn

Qiang Du
qd2125@columbia.edu

[1] Department of Applied Physics and Applied Mathematics, Columbia University, New York, NY 10027, USA

[2] Hubei Key Laboratory of Mathematical Sciences & School of Mathematics and Statistics, Central China Normal University, Wuhan 430079, China

of integro-differential equations. More recently, mathematical analysis of nonlocal models is also paid more attention, which could be found in [2–4,9,17,20,21]. Meanwhile, to simulate nonlocal models, various numerical approximations have been proposed and studied, including finite difference, finite element, meshfree method, quadrature and particle-based methods [7,10,18,22,23,25,27,33–37,39]. For a more recent review, we refer to [15].

Let $\Omega \subset \mathbb{R}^d$ denote a bounded, open and convex domain with Lipschitz continuous boundary. For $u(\mathbf{x}) : \Omega \to \mathbb{R}$, the nonlocal operator $\mathcal{L}$ on $u(\mathbf{x})$ is defined as

$$\mathcal{L}u(\mathbf{x}) = \int_{\mathbb{R}^d} \big(u(\mathbf{y}) - u(\mathbf{x})\big)\gamma(\mathbf{x}, \mathbf{y})d\mathbf{y} \qquad \forall \mathbf{x} \in \Omega, \tag{1}$$

where the nonnegative symmetric mapping $\gamma(\mathbf{x}, \mathbf{y}) : \mathbb{R}^d \times \mathbb{R}^d \to \mathbb{R}$ is called a kernel. The operator $\mathcal{L}$ is regarded nonlocal since the value of $\mathcal{L}u$ at a point $\mathbf{x}$ involves information about u at points $\mathbf{y} \neq \mathbf{x}$. In this article, we consider the following nonlocal Dirichlet volume-constrained diffusion problem

$$\begin{cases} -\mathcal{L}u(\mathbf{x}) = b(\mathbf{x}) & \text{on } \Omega, \\ u(\mathbf{x}) = g(\mathbf{x}) & \text{on } \Omega_I, \end{cases} \tag{2}$$

where $\Omega_I = \{\mathbf{y} \in \mathbb{R}^d \setminus \Omega : \text{dist}(\mathbf{y}, \partial\Omega) < \delta\}$ with δ a constant called horizon parameter, $b(\mathbf{x}) \in L^2(\Omega)$ and $g(\mathbf{x}) \in L^2(\Omega_I)$ are given functions. Nonlocal volumetric constraints are natural extensions, to the nonlocal case, of local boundary conditions for differential equation problems. Nonlocal versions of Neumann and Robin boundary conditions are also naturally defined [15,16,32].

In this work, the nonnegative symmetric kernel $\gamma(\mathbf{x}, \mathbf{y})$ is assumed to satisfy the following conditions:

$$\begin{cases} \forall \mathbf{x} \in \Omega \cup \Omega_I, \quad \text{there exists a constant} \gamma_0 > 0 \quad \text{such that:} \\ \gamma(\mathbf{x}, \mathbf{y}) \geq \gamma_0, \quad \forall \mathbf{y} \in B_{\delta/2}(\mathbf{x}), \quad \text{and } \gamma(\mathbf{x}, \mathbf{y}) = 0, \quad \forall \mathbf{y} \in (\Omega \cup \Omega_I) \setminus B_\delta(\mathbf{x}). \\ \text{Moreover,} \quad \gamma(\mathbf{x}, \mathbf{y}) = \tilde{\gamma}(|\mathbf{y} - \mathbf{x}|), \quad \text{with } \int_{\mathbb{R}^d} \tilde{\gamma}(|\mathbf{z}|)d\mathbf{z} = 1. \end{cases} \tag{3}$$

Here $B_\delta(\mathbf{x}) := \{\mathbf{y} \in \Omega \cup \Omega_I : |\mathbf{y} - \mathbf{x}| \leq \delta\}$. This implies that nonlocal interactions are radially symmetric and limited to a spherical neighborhood of radius δ. Moreover, we may also write $\gamma(\mathbf{x}, \mathbf{y}) = \gamma(\mathbf{x} - \mathbf{y})$ to utilize the translation invariance. A few important classes of kernels are considered in [16]. This condition (3) on γ implies that $\mathcal{L}$ is a bounded mapping from $L^2(\mathbb{R}^d)$ to $L^2(\mathbb{R}^d)$. Such a case has also been studied earlier in [4].

As to be discussed later, for smooth enough $b(\mathbf{x})$ in Ω, the solution $u(\mathbf{x})$ could possibly be discontinuous across $\partial\Omega$, which makes the numerical solution to the corresponding nonlocal problem challenging. An intuitive idea to overcome the possible loss of continuity is to use discontinuous Galerkin (DG) methods and it could be conforming, which is in stark contrast to DG methods for the discretization of second order elliptic partial differential equations for which they are always nonconforming [5]. While nonconforming DG has also been studied recently for nonlocal models [12], if the structure of the solution could be studied carefully, a well designed conforming DG method could be a more competitive option as it could lessen the cost of computation. In this work, we propose a new kind of conforming DG method to approximate the nonlocal problem (2) with kernels satisfying (3) where the key is to adopt a hybrid version of continuous elements with DG at $\partial\Omega$. The new method enjoys various advantages on both theory and practice. Careful estimates show that they are optimal under very reasonable regularity assumptions. The theory is also numerically verified through computational experiments.

The paper is organized as follows. In Sect. 2, the structure of the solution for the given problem is analyzed, which is a generalization of the results in [30]. Since the original

inhomogeneous problem (2) is converted into the homogeneous problem (5), so we just need to discuss homogeneous problem (6) with a smoother right hand side function. Based on the structure of the solution, in Sect. 3 we propose a new DG method which solves the problem (6) efficiently. Convergence analysis and condition number estimates along with asymptotic compatibility for the method are given in Sect. 4. Results of numerical experiments are reported in Sect. 5.

2 The Structure of the Solution

To design more efficient numerical discretization, we first present some regularity studies on the nonlocal constrained value problem. We recall first some one dimensional (1D) results presented in [30]: when using peridynamic theory to model the elasticity on $\mathbb{R} = (-\infty, \infty)$, the displacement field u has the same smoothness as the body force field b. In addition, any discontinuity in the kernel γ (or in one of its derivatives) has some additional effect on the smoothness of u. For a peridynamic bar, suppose that b has a discontinuity in its Nth derivative at some $x = x_b$, and γ has a discontinuity in its Lth derivative at some $x = x_c$, then u has a discontinuity in its $(N + nL + n)$th derivative at $x = x_b + nx_c$, $n = 1, 2, \ldots$. This propagation of discontinuities is illustrated schematically in [30, Figure 3]. Roughly speaking, the smoothness of u increases as one moves away from the location where the solution is discontinuous due to the discontinuity of the body force field b. These types of step-wise improved regularity associated with a finite horizon parameter have also been observed for nonlocal initial value problems of nonlocal-in-time dynamic systems in [13]. For the nonlocal problem with its kernel function satisfying (3) in a bounded domain, the authors in [16] have proved the conclusion that $u(\mathbf{x}) \in L^2(\Omega \cup \Omega_I)$, which is insufficient for investigating efficient and effective numerical approximation.

Recall result for 1D case on $\mathbb{R}$, the regularity of the solution for a nonlocal problem is affected by both the right hand side function and the kernel function, assuming good behavior of the solution at infinities. In this section we consider the effect from these two sources on the regularity on the solution for general multidimensional constrained value problem on a bounded domain.

First, let us present a result to reduce the problem (2) under consideration to a problem with a homogeneous nonlocal constraint. Denoted by

$$\overline{b}(\mathbf{x}) = \begin{cases} b(\mathbf{x}), & \mathbf{x} \in \Omega, \\ g(\mathbf{x}), & \mathbf{x} \in \Omega_I, \end{cases}$$

and

$$\overline{u}(\mathbf{x}) = u(\mathbf{x}) - \overline{b}(\mathbf{x}). \tag{4}$$

Then the nonlocal operator $-\mathcal{L}$ on $\overline{u}(\mathbf{x})$ is

$$\begin{aligned} -\mathcal{L}\overline{u}(\mathbf{x}) = f(\mathbf{x}) &= \int_{B_\delta(\mathbf{x})} \overline{b}(\mathbf{y})\gamma(\mathbf{y}-\mathbf{x})d\mathbf{y} \\ &= \int_{B_\delta(\mathbf{x})\cap\Omega} b(\mathbf{y})\gamma(\mathbf{y}-\mathbf{x})d\mathbf{y} + \int_{B_\delta(\mathbf{x})\cap\Omega_I} g(\mathbf{y})\gamma(\mathbf{y}-\mathbf{x})d\mathbf{y}, \quad \forall \mathbf{x} \in \Omega. \end{aligned}$$

Thus, $\overline{u}(\mathbf{x})$ is the solution of the following homogeneous nonlocal problem

$$\begin{cases} -\mathcal{L}\overline{u}(\mathbf{x}) = f(\mathbf{x}), & \text{on } \Omega, \\ \overline{u}(\mathbf{x}) = 0, & \text{on } \Omega_I. \end{cases} \tag{5}$$

If $\gamma(\mathbf{s}) \in L^2(\mathbb{R}^d)$, then due to the fact that the convolution of functions in dual $L^p(\mathbb{R}^d)$-spaces is continuous, we know that $f(\mathbf{x}) \in C(\Omega)$. On the other hand, by only assuming that $\gamma(\mathbf{s}) \in L^1(\mathbb{R}^d)$, in order to assure $f(\mathbf{x}) \in C(\Omega)$, we need the condition $b(\mathbf{x}) \in L^\infty(\Omega)$ and $g(\mathbf{x}) \in L^\infty(\Omega_I)$.

The problem (2) is equivalent via (4) to the problem (5) which has a homogeneous nonlocal constraint. That is, we just need to study the following homogeneous nonlocal problem:

$$\begin{cases} -\mathcal{L}u(\mathbf{x}) = b(\mathbf{x}), & \text{on } \Omega, \\ u(\mathbf{x}) = 0, & \text{on } \Omega_I, \end{cases} \tag{6}$$

with $b(\mathbf{x}) \in C(\Omega)$, $\gamma(\mathbf{x}, \mathbf{y})$ satisfying (3). We will show that if $\gamma(\mathbf{x}, \mathbf{y})$ satisfies some additional mild assumptions, the regularity results recalled earlier for the 1D case can be generalized to multidimensional case on a bounded domain.

Theorem 1 *If $\gamma(\mathbf{x}, \mathbf{y})$ satisfies (3), and $b(\mathbf{x}) \in C(\Omega)$, the solution of (6) is continuous in Ω, i.e., $u(\mathbf{x}) \in C(\Omega)$.*

Proof Since $\gamma(\mathbf{x}, \mathbf{y})$ satisfies (3), if $b(\mathbf{x}) \geq 0 \ \forall \mathbf{x} \in \Omega$, then

$$u(\mathbf{x}) \geq \int_{B_\delta(\mathbf{x})} u(\mathbf{y})\gamma(\mathbf{y} - \mathbf{x})d\mathbf{y} \quad \forall \mathbf{x} \in \Omega.$$

This means the nonlocal Eq. (6) satisfies the maximum principle, due to the condition $b(\mathbf{x}) \in C(\Omega)$ and $u(\mathbf{x}) = 0$ on Ω_I, we get that

$$u(\mathbf{x}) \in L^\infty(\Omega \cup \Omega_I).$$

From (6), we have

$$u(\mathbf{x}) = b(\mathbf{x}) + \int_{B_\delta(\mathbf{x})} u(\mathbf{y})\gamma(\mathbf{y} - \mathbf{x})d\mathbf{y}, \quad \forall \mathbf{x} \in \Omega.$$

Since $u(\mathbf{x}) \in L^\infty(\Omega \cup \Omega_I)$ and $\gamma(\mathbf{s}) \in L(\mathbb{R}^d)$, thus

$$\int_{B_\delta(\mathbf{x})} u(\mathbf{y})\gamma(\mathbf{y} - \mathbf{x})d\mathbf{y}$$

is continuous for $\mathbf{x}$ in Ω. Together with the condition $b(\mathbf{x}) \in C(\Omega)$, we complete the proof. □

With regard to the maximum principle used in the above proof, we refer to [31,33] for additional discussions. With an additional assumption on the kernel, we can bootstrap a higher order regularity result as follows.

Theorem 2 *Suppose that $\gamma(\mathbf{x}, \mathbf{y})$ satisfies (3). If $b(\mathbf{x}) \in C^1(\Omega)$, $\tilde{\gamma}(r) \in W^{1,1}(0, \delta)$ and $\tilde{\gamma}(\delta) = 0$, then $u(\mathbf{x}) \in C^1(\Omega)$. Furthermore, if $d \geq 2$ and $\partial\Omega \cap B_\delta(\mathbf{x})$ is measure zero for all $\mathbf{x} \in \Omega$, the condition $\tilde{\gamma}(\delta) = 0$ could be dropped.*

Proof From (6), we know

$$u(\mathbf{x}) = b(\mathbf{x}) + \int_{B_\delta(\mathbf{0})} u(\mathbf{x} + \mathbf{s})\gamma(\mathbf{s})d\mathbf{s}. \tag{7}$$

For any unit vector $\mathbf{t}$, we take the corresponding directional derivative for (7), so

$$\frac{\partial u(\mathbf{x})}{\partial \mathbf{t}} = \frac{\partial b(\mathbf{x})}{\partial \mathbf{t}} + \int_{B_\delta(\mathbf{0})} \frac{\partial u(\mathbf{x} + \mathbf{s})}{\partial \mathbf{t}}\gamma(\mathbf{s})d\mathbf{s}.$$

Using the divergence theorem, since $\tilde{\gamma}(r) \in W^{1,1}(0,\delta)$, thus with well-defined $\tilde{\gamma}(\delta)$, we have

$$\begin{aligned}
&\int_{B_\delta(\mathbf{0})} \frac{\partial u(\mathbf{x}+\mathbf{s})}{\partial \mathbf{t}} \gamma(\mathbf{s}) d\mathbf{s} \\
&= \int_{\partial B_\delta(\mathbf{0})} u(\mathbf{x}+\mathbf{s})\gamma(\mathbf{s})\mathbf{t}\cdot\mathbf{n}_\mathbf{s} d\mathbf{S}_\mathbf{s} - \int_{B_\delta(\mathbf{0})} u(\mathbf{x}+\mathbf{s})\mathbf{t}\cdot\nabla\gamma(\mathbf{s}) d\mathbf{s} \\
&= \tilde{\gamma}(\delta)\int_{\partial B_\delta(\mathbf{0})} u(\mathbf{x}+\mathbf{s})\mathbf{t}\cdot\mathbf{n}_\mathbf{s} d\mathbf{S}_\mathbf{s} - \int_{B_\delta(\mathbf{0})} u(\mathbf{x}+\mathbf{s})\tilde{\gamma}'(|\mathbf{s}|)\mathbf{t}\cdot\mathbf{n}_\mathbf{s} d\mathbf{s}
\end{aligned}$$

So

$$\frac{\partial u(\mathbf{x})}{\partial \mathbf{t}} = \frac{\partial b(\mathbf{x})}{\partial \mathbf{t}} + \tilde{\gamma}(\delta)\int_{\partial B_\delta(\mathbf{0})} u(\mathbf{x}+\mathbf{s})\mathbf{t}\cdot\mathbf{n}_\mathbf{s} d\mathbf{S}_\mathbf{s} - \int_{B_\delta(\mathbf{0})} u(\mathbf{x}+\mathbf{s})\tilde{\gamma}'(|\mathbf{s}|)\mathbf{t}\cdot\mathbf{n}_\mathbf{s} d\mathbf{s} \tag{8}$$

If $\tilde{\gamma}(\delta) = 0$, we have

$$\frac{\partial u(\mathbf{x})}{\partial \mathbf{t}} = \frac{\partial b(\mathbf{x})}{\partial \mathbf{t}} - \int_{B_\delta(\mathbf{0})} u(\mathbf{x}+\mathbf{s})\tilde{\gamma}'(|\mathbf{s}|)\mathbf{t}\cdot\mathbf{n}_\mathbf{s} d\mathbf{s}. \tag{9}$$

Since the convolution of functions in dual $L^p(\mathbb{R}^d)$-spaces is continuous, the second term in the right hand side of (9) is continuous with respect to $\mathbf{x}$. Together with the condition $b(\mathbf{x}) \in C^1(\Omega)$, we have $u(\mathbf{x}) \in C^1(\Omega)$. If $d \geq 2$ and $\partial\Omega \cap B_\delta(\mathbf{x})$ is measure zero for all $\mathbf{x} \in \Omega$, the second term in (8)

$$\tilde{\gamma}(\delta)\int_{\partial B_\delta(\mathbf{0})} u(\mathbf{x}+\mathbf{s})\mathbf{t}\cdot\mathbf{n}_\mathbf{s} d\mathbf{S}_\mathbf{s}$$

is continuous with respect to $\mathbf{x}$, thus we complete the proof. □

We want to point out that for $d \geq 2$ the condition "$\partial\Omega \cap B_\delta(\mathbf{x})$ is measure zero for all $\mathbf{x} \in \Omega$" is generally satisfied except for some special cases, such as

$$\Omega = B_1(\mathbf{0}),\ \delta = 1,$$

where $\partial\Omega \cap B_\delta(\mathbf{0}) = \partial\Omega$ and $\partial\Omega \cap B_\delta(\mathbf{x})$ is measure zero for any $\mathbf{x} \in \Omega \setminus \{\mathbf{0}\}$.

From (9) we get that under the assumptions of Theorem 2, if the first derivative of the right hand side b is discontinuous at some point $\mathbf{x}$, the first derivative of the solution u will be discontinuous at the same point. However, if we may have both the condition $\tilde{\gamma}(\delta) > 0$ and the condition $b(\mathbf{x}) \notin C^1(\Omega)$, the conclusion $u(\mathbf{x}) \in C^1(\Omega)$ may still hold, see Example 1, where in fact $u(\mathbf{x}) \in C^\infty(\Omega)$. This is not contradicting as *the sum of two discontinuous function could be continuous, and even infinitely differentiable*.

For the convenience of following discussion, let us denote by

$$\Omega_1 = \{\mathbf{x} \in \Omega : \mathrm{dist}(x, \partial\Omega) > \delta\} \quad \text{and} \quad \Omega_2 = \Omega \setminus \overline{\Omega_1}. \tag{10}$$

We now explain the significance of Theorem 1, which is stated in twofold as follows. First, it indicates that *the smoothness of $u(\mathbf{x})$ is the same as $b(\mathbf{x})$ for problems on general multidimensional bounded domains*. Second, it reveals the possible propagation of discontinuities due to the kernel. Although $b(\mathbf{x}) \in C(\Omega)$, it might be discontinuous across $\partial\Omega$. So does $u(\mathbf{x})$, and this discontinuity will propagate to those points on $\partial\Omega_1$, where u enjoys one order higher derivatives, which is consistent with the conclusion for 1D case on $\mathbb{R}$ with $N = 0$ and $L = 0$. Similar argument can be given for Theorem 2 which is consistent with the conclusion for 1D case on $\mathbb{R}$ with $N = 0$ and $L = 1$. This bootstrap procedure could be repeated again and again, and the corresponding results for general N and L then follow.

Let us now discuss the importance and necessity of the smoothness for the kernel function in 1D case. Without loss of generality, let $\Omega = (0, 1)$. For instance, $\tilde{\gamma}(\delta) = 0$ in Theorem 2 is required. If this condition does not hold, from the proof of the Theorem 2, we see that $u(x) \in C^1(\Omega)$ may not hold. In fact, since

$$u'(x) = b'(x) + \tilde{\gamma}(\delta)\big(u(x+\delta) - u(x-\delta)\big) - \int_{-\delta}^{\delta} u(x+s)\tilde{\gamma}'(|s|)ds,$$

if $\tilde{\gamma}(\delta) > 0$ and u is discontinuous at $x = 0$ or $x = 1$, then the term

$$\tilde{\gamma}(\delta)\big(u(x+\delta) - u(x-\delta)\big)$$

is likely to be discontinuous at $x = \delta$ or $x = 1-\delta$. In such case, $u'(x)$ would be discontinuous at these points. This situation might happen, as illustrated in Example 2. Using a similar argument we could prove the following theorem.

Theorem 3 *Suppose $\gamma(\mathbf{x}, \mathbf{y})$ satisfies (3). If the following conditions hold:*

(i) $b(\mathbf{x}) \in C^1(\Omega) \cap C^2(\Omega_1) \cap C^2(\Omega_2)$,
(ii) $\tilde{\gamma}(r) \in W^{1,1}(0, \delta)$ *and* $\tilde{\gamma}(\delta) = 0$.

Then $u \in C^1(\Omega) \cap C^2(\Omega_1) \cap C^2(\Omega_2)$. Furthermore, if $d \geq 2$ and $\partial\Omega \cap B_\delta(\mathbf{x})$ is measure zero for all $\mathbf{x} \in \Omega$, the condition $\tilde{\gamma}(\delta) = 0$ could be dropped.

Proof The conditions of Theorem 2 hold due to the conditions (i) and (ii), so $u \in C^1(\Omega)$. Furthermore, for any two unit vectors $\mathbf{t}_1$ and $\mathbf{t}_2$, take a directional derivative for (9), we get

$$\frac{\partial^2 u(\mathbf{x})}{\partial \mathbf{t}_1 \partial \mathbf{t}_2} = \frac{\partial^2 b(\mathbf{x})}{\partial \mathbf{t}_1 \partial \mathbf{t}_2} - \int_{B_\delta(\mathbf{0})} \frac{\partial u(\mathbf{x}+\mathbf{s})}{\partial \mathbf{t}_2} \tilde{\gamma}'(|\mathbf{s}|)\mathbf{t}_1 \cdot \mathbf{n}_\mathbf{s} d\mathbf{s}.$$

Applying this equality in Ω_1 and Ω_2 will lead to the conclusion $u \in C^2(\Omega_1)$ and $u \in C^2(\Omega_2)$, respectively. □

To get the optimal convergence rate for the linear finite element method (FEM), we always need the regularity $u \in H^2(\Omega)$, the following theorem give a sufficient condition to guarantee this property.

Theorem 4 *Suppose $\gamma(\mathbf{x}, \mathbf{y})$ satisfies (3) and the following conditions hold:*

(i) $b(\mathbf{x}) \in C^1(\Omega) \cap H^2(\Omega_1) \cap H^2(\Omega_2)$,
(ii) $\tilde{\gamma}(r) \in W^{1,1}(0, \delta)$ *and* $\tilde{\gamma}(\delta) = 0$.

Then $u \in H^2(\Omega)$. Furthermore, if $d \geq 2$ and $\partial\Omega \cap B_\delta(\mathbf{x})$ is measure zero for all $\mathbf{x} \in \Omega$, the condition $\tilde{\gamma}(\delta) = 0$ could be dropped.

Proof Using the density of $C^2(\Omega_i)$ in $H^2(\Omega_i)$ $(i = 1, 2)$ and Theorem 3 we get the result $u \in H^2(\Omega_i)$. Since $u \in C^1(\Omega)$ is proven, the result $u \in H^2(\Omega)$ holds. □

3 A New DG Method for Nonlocal Models with Integrable Kernels

Here we denote by $\mathbf{n}_\mathbf{x}$ the outward normal derivative at point $\mathbf{x}$. Under the condition of Theorem 1, we know that for given $\mathbf{x} \in \partial\Omega$,

$$\lim_{h \to 0+} u(\mathbf{x} + h\mathbf{t}) = \lim_{h \to 0-} u(\mathbf{x} + h\mathbf{n}_\mathbf{x}), \quad \forall \mathbf{t} \cdot \mathbf{n}_\mathbf{x} < 0.$$

However it is not necessarily zero, that is $u(\mathbf{x})$ is possibly discontinuous across $\partial\Omega$. Thus, it might be inefficient to use continuous FEM on the whole domain $\Omega \cup \Omega_I$. Moreover, since we do not specify the value of the right hand side function on Ω_I a priori, we have no control on the amount of the jump across $\partial\Omega$ where the solution is likely to be discontinuous. Based on these consideration, in this paper we propose a suitable DG method by adopting a hybrid version of DG (across the domain boundary) and continuous elements (in the interior domain).

As in [16] the nonlocal energy inner product, the nonlocal energy norm, nonlocal energy space, and nonlocal volume constrained energy space are defined by

$$(u, v)_{|||} := \Big(\int_{\Omega\cup\Omega_I} \int_{\Omega\cup\Omega_I} \big(u(\mathbf{y}) - u(\mathbf{x})\big)\big(v(\mathbf{y}) - v(\mathbf{x})\big)\gamma(\mathbf{x}, \mathbf{y}) d\mathbf{y} d\mathbf{x}\Big),$$

$$|||u||| := (u, u)_{|||}^{1/2},$$

$$V(\Omega \cup \Omega_I) := \{u \in L^2(\Omega \cup \Omega_I) : |||u||| < \infty\},$$

$$V_{c,0}(\Omega \cup \Omega_I) := \{u \in V(\Omega \cup \Omega_I) : u(\mathbf{x}) = 0 \text{ on } \Omega_I\},$$

respectively. Similar to the definition $V_{c,0}(\Omega \cup \Omega_I)$, the subspace of $L^2(\Omega \cup \Omega_I)$ is defined as follows:

$$L^2_{c,0}(\Omega \cup \Omega_I) := \{u \in L^2(\Omega \cup \Omega_I) : u(\mathbf{x}) = 0 \text{ on } \Omega_I\}.$$

The authors in [16] prove that if the kernel function $\gamma(\mathbf{x}, \mathbf{y})$ satisfies (3), then $V_{c,0}(\Omega \cup \Omega_I)$ is equivalent to $L^2_{c,0}(\Omega \cup \Omega_I)$. Denote by

$$V^{pc}_{c,0}(\Omega \cup \Omega_I) = \{u \in V_{c,0}(\Omega \cup \Omega_I) : u|_\Omega \in C(\Omega)\},$$

where the superscripts pc means *partly continuous* (continuous in Ω).

We now describe the triangulation $\mathcal{T}_h$ of $\Omega \cup \Omega_I$ for two dimensional (2D) case. First the domain Ω is approximated by a domain Ω_h with a polygonal boundary Γ_h whose vertices all lie on $\partial\Omega$. Let Ω_{Ih} be the domain with $\partial(\Omega \cup \Omega_I)$ and Γ_h as its exterior and interior boundaries, respectively, see Fig. 2 in [11]. The triangulation $\mathcal{T}_h$ composes of a finite set of closed triangles $\mathcal{T}_h = \{K\}$ which satisfied the conditions (A1)–(A3) ([11]). Since the conditions (A1) and (A2) are standard requirements in finite element field, here we just list the condition (A3):

(A3) each $K \in \mathcal{T}_h$ is either in Ω_h and Ω_{Ih}, and has at most two vertices lying on Γ_h.

We call this kind of triangulation $\mathcal{T}_h$ as conforming with the boundary $\partial\Omega$.

Next, let $V^{pc,h}_{c,0}$ consist of those functions in $V^{pc}_{c,0}(\Omega \cup \Omega_I)$ that are piecewise linear. Since Ω is convex, the following conforming property is satisfied,

$$V^{pc,h}_{c,0} \subset V^{pc}_{c,0}(\Omega \cup \Omega_I). \tag{11}$$

Remark 1 Here we use piecewise linear function, similar discussion could be given for higher order finite element spaces. However, since u is often not so smooth, e.g. $u \in H^s(\Omega)$ with $s < 2$, or under some conditions $s = 2$. Using high order finite element spaces could not improve the convergence rate in these cases.

We assume that $\mathcal{T}_h$ is shape-regular and quasi-uniform [8] as $h \to 0$, where h denotes the diameter of the largest element in $\mathcal{T}_h$. For a fixed $\mathcal{T}_h$, the set of inner nodes of Ω_h, i.e., all nodes in $\Omega_h \setminus \partial\Omega$, is denoted by $NI = \{\mathbf{x}_j : j = 1, 2, \ldots, m\}$, with piecewise linear basis functions defined on $\mathcal{T}_h$ being $\phi_j(\mathbf{x})$, $j = 1, 2, \ldots, m$. The set of all nodes in Γ_h is

denoted by $NB = \{\mathbf{x}_{m+j} : j = 1, 2, \ldots, n\}$ with piecewise linear basis functions defined on $\mathcal{T}_h$ being $\phi_{m+j}(\mathbf{x}),\ j = 1, 2, \ldots, n$. The basis functions for the space $V_{c,0}^{pc,h}$ are as follows: for $j = 1, 2, \ldots, m+n$,

$$\widehat{\phi}_j(\mathbf{x}) = \begin{cases} \phi_j(\mathbf{x})|_{\Omega_h}, & \mathbf{x} \in \Omega_h, \\ 0, & \mathbf{x} \in (\Omega \cup \Omega_I) \setminus \Omega_h. \end{cases}$$

Throughout the paper, the generic constant C is always independent of the finite element mesh parameter h.

Since we know the structure of the true solution and the space it belongs to, we could design a DG method for its approximation. First, variational form in $V_{c,0}^{pc}(\Omega \cup \Omega_I)$ finds $u(\mathbf{x}) \in V_{c,0}^{pc}(\Omega \cup \Omega_I)$, such that

$$-\int_{\Omega} \mathcal{L}u(\mathbf{x})w(\mathbf{x})d\mathbf{x} = \int_{\Omega} b(\mathbf{x})w(\mathbf{x})d\mathbf{x},\ \forall w(\mathbf{x}) \in V_{c,0}^{pc}(\Omega \cup \Omega_I). \tag{12}$$

The finite dimensional approximation for (12) finds $u_h(\mathbf{x}) \in V_{c,0}^{pc,h}$, such that

$$-\int_{\Omega_h} \mathcal{L}u_h(\mathbf{x})w_h(\mathbf{x})d\mathbf{x} = \int_{\Omega_h} b(\mathbf{x})w_h(\mathbf{x})d\mathbf{x},\ \forall w_h(\mathbf{x}) \in V_{c,0}^{pc,h}. \tag{13}$$

Set $u_h(\mathbf{x}) = \sum_{j=1}^{m+n} u_j \widehat{\phi}_j(\mathbf{x})$, $\mathbf{u} = (u_1, u_2, \ldots, u_{m+n})^T$. Denote by

$$\mathbf{d} = (d_1, d_2, \ldots, d_{m+n})^T,$$

and

$$A_{II} = (a_{i,j})_{m\times m},\ A_{IB} = (a_{i,m+j})_{m\times n},\ A_{BB} = (a_{m+i,m+j})_{n\times n},$$

with

$$d_i = \int_{\Omega_h} b(\mathbf{x})\widehat{\phi}_i(\mathbf{x})d\mathbf{x},\ a_{i,j} = -\int_{\Omega_h} \mathcal{L}\widehat{\phi}_j(\mathbf{x})\widehat{\phi}_i(\mathbf{x})d\mathbf{x}.$$

Set $w_h = \widehat{\phi}_i$, $i = 1, 2, \ldots, m+n$, the algebraic system of (13) is

$$A\mathbf{u} = \mathbf{d},$$

with

$$A = \begin{pmatrix} A_{II} & A_{IB} \\ A_{IB}^T & A_{BB} \end{pmatrix}. \tag{14}$$

Here we use the finite element space $V_{c,0}^{pc,h}$ which is continuous in Ω_h, however, discontinuous across $\partial\Omega_h$, thus we regard it a conforming but hybrid version of DG and continuous FEM. This method possesses some advantages as follows:

(i) The method leads to a linear algebraic system with the coefficient matrix A in (14) that is symmetric and positive definite, just as in the case using either the conforming DG or continuous FEM, thus many efficient solvers suitable to such linear systems could still be used.

(ii) The method is asymptotically compatible as long as $\mathcal{T}_h$ is conforming with the $\partial\Omega$. In this case, as shown in [34], as long as the finite element space contains continuous piecewise linear functions (which is the case for our hybrid algorithm), the Galerkin finite element approximation is always asymptotically compatible, and thus offers robust numerical discretizations to problems involving nonlocal interactions.

(iii) The method has optimal convergence rate provided that the solution is smooth in Ω, that is $O(h^2)$ for error in L^2 norm provided that the true solution $u \in H^2(\Omega)$, see Theorem 6. This result is in sharp contrast to the assumption given that in [16] where to insure the optimal convergence rate the true solution is required to be in $H^2(\Omega \cup \Omega_I)$ which generally not holds for the problem (6). Furthermore, it has optimal convergence rate for any dimensional case under mild assumptions, see Theorem 6 and 7 .

(iv) The method, in comparison with the direct use of DG in all discrete elements, yields a smaller system with smaller degree of freedoms. For example, the degree of freedoms is $n+1$ versus $2n$ for a mesh with $n+1$ nodes in 1D case, and $(n+1)^2$ versus $6n^2$ for a uniform triangulation with n^2 nodes in 2D case.

4 Theoretical Analysis

We now provide further theoretical analysis on the new DG approximations. Given what has already been discussed in (ii) of the above section, the asymptotic compatibility is assured as $\delta \to 0$, and we thus focus on the case where the problems remain strictly nonlocal with a finite and fixed $\delta > 0$.

4.1 Convergence Analysis for General Dimensional Case

The following convergence result describes the best approximation property of the finite-dimensional Ritz–Galerkin solution.

Theorem 5 *If $\gamma(\mathbf{x}, \mathbf{y})$ satisfies (3), $b(\mathbf{x}) \in C(\Omega)$, $u(\mathbf{x})$ is the solution of (6), $u_h(\mathbf{x})$ is the solution of (13). We define*

$$\tilde{u}(\mathbf{x}, \Omega_h) = \begin{cases} u(\mathbf{x}), & \mathbf{x} \in \Omega_h, \\ 0, & \mathbf{x} \in (\Omega \cup \Omega_I) \setminus \Omega_h. \end{cases}$$

Then we have

$$\|\|\tilde{u} - u_h\|\| \leq \inf_{w_h \in V_{c,0}^{pc,h}} \|\|\tilde{u} - w_h\|\|. \tag{15}$$

Consequently,

$$\|u - u_h\|_{\Omega_h} \leq C \min_{w_h \in V_{c,0}^{pc,h}} \|u - w_h\|_{\Omega_h} \to 0 \quad as\ h \to 0. \tag{16}$$

Proof Since $V_{c,0}^{pc,h} \subset V_{c,0}^{pc}(\Omega \cup \Omega_I)$ as in (11), then for all $w_h \in V_{c,0}^{pc,h}$,

$$-\int_{\Omega_h} \mathcal{L}\tilde{u}(\mathbf{x}, \Omega_h) w_h(\mathbf{x}) d\mathbf{x} = \int_{\Omega_h} b(\mathbf{x}) w_h(\mathbf{x}) d\mathbf{x},$$

together with (13), we have

$$-\int_{\Omega_h} \mathcal{L}\big(\tilde{u}(\mathbf{x}, \Omega_h) - u_h(\mathbf{x})\big) w_h(\mathbf{x}) d\mathbf{x} = 0, \quad \forall w_h \in V_{c,0}^{pc,h}.$$

Using the nonlocal Green's first identity [17], we have

$$(\tilde{u} - u_h, w_h)_{|||} = 0, \quad \forall w_h \in V_{c,0}^{pc,h}.$$

Then we get the following estimate

$$\begin{aligned} |||\tilde{u} - u_h|||^2 &= (\tilde{u} - u_h, \tilde{u} - u_h)_{|||} = (\tilde{u} - u_h, \tilde{u} - w_h)_{|||} \\ &\le |||\tilde{u} - u_h||| |||\tilde{u} - w_h|||, \quad \forall w_h(\mathbf{x}) \in V_{c,0}^{pc,h}, \end{aligned}$$

and then

$$|||\tilde{u} - u_h||| \le |||\tilde{u} - w_h|||, \quad \forall w_h(\mathbf{x}) \in V_{c,0}^{pc,h}.$$

By the equivalence between $V_{c,0}(\Omega \cup \Omega_I)$ and $L_{c,0}^2(\Omega \cup \Omega_I)$ ([16]), we complete the proof. □

Let us note that due to the use of norm equivalence in the above proof, generally speaking, the constant C in the lemma could depend on the nonlocal space and thus the nonlocal kernel. One may not infer that this constant remains uniformly bounded when we consider the local limit of the nonlocal problem. Fortunately, as alluded to earlier, with the asymptotic compatibility already established in [34], we hereby only focus on the strict nonlocal case.

We now combine the theory of the interpolation error estimate and (16) to give the convergence rate estimate.

Theorem 6 *If $\gamma(\mathbf{x}, \mathbf{y})$ satisfies (3), $b(\mathbf{x}) \in C(\Omega)$, $u(\mathbf{x})$ is the solution of (6), $u_h(\mathbf{x})$ is the solution of (13). Suppose that $u \in H^t(\Omega)$ holds, there exists a constant C such that, for sufficiently small h,*

$$\|u - u_h\|_{\Omega_h} \le Ch^s \|u\|_{s,\Omega}, \tag{17}$$

with $s = \min(t, 2) > d/2$. If $s > 1$

$$\|\nabla(u - u_h)\|_{\Omega_h} \le Ch^{s-1} \|u\|_{s,\Omega}. \tag{18}$$

Moreover, if the conditions of Theorem 4 hold, we get $u \in H^2(\Omega)$, thus $s = 2$.

Proof Denote by $\mathcal{I}_h u$ the Lagrange interpolant from $C(\Omega_h)$ to $V_{c,0}^{pc,h}|_{\Omega_h}$, and

$$w_h(\mathbf{x}) = \begin{cases} \mathcal{I}_h u(\mathbf{x}), & \mathbf{x} \in \Omega_h, \\ 0, & \mathbf{x} \in (\Omega \cup \Omega_I) \setminus \Omega_h, \end{cases}$$

then $w_h \in V_{c,0}^{pc,h}$, and

$$\|u - w_h\|_{\Omega_h} = \|u - \mathcal{I}_h u\|_{\Omega_h} \le Ch^s \|u\|_{s,\Omega}, \tag{19}$$

with $s = \min(t, 2)$. Combination of (16) and (19) leads to (17).

Using the inverse estimate for finite element space, we have

$$\begin{aligned} \|\nabla(u - u_h)\|_{\Omega_h} &\le \|\nabla(\mathcal{I}_h u - u_h)\|_{\Omega_h} + \|\nabla(u - \mathcal{I}_h u)\|_{\Omega_h} \\ &\le Ch^{-1} \|\mathcal{I}_h u - u_h\|_{\Omega_h} + Ch^{s-1} \|u\|_{s,\Omega} \le Ch^{s-1} \|u\|_{s,\Omega} \end{aligned}$$

This is the desired result (18). □

We recall by Theorem 6.2 in [16] that, when continuous FEM is used to approximate the nonlocal problem (6), the approximation u_n has an error estimate of the form $\|u-u_n\|_{\Omega\cup\Omega_I} \leq Ch^s\|u\|_{s,\Omega\cup\Omega_I}$. Since the solution of nonlocal problem (6) could be discontinuous across $\partial\Omega$, we see that $u \in H^s(\Omega\cup\Omega_I)$ does not hold for $s \geq 1/2$, let alone for $s = 2$. For $d \geq 2$, if the conditions of Theorem 4 (for such case we need the condition $\partial\Omega \cap B_\delta(\mathbf{x})$ is measure zero for all $\mathbf{x} \in \Omega$, however do not need the condition $\tilde{\gamma}(\delta) = 0$) are satisfied, the optimal convergence rate will be gained for our DG method.

For 1D case, if the condition (i) and (ii) of Theorem 4 are satisfied, the optimal convergence rate will also be gained for our DG method. However, the condition (ii) is so strong that many kernel functions do not satisfy. For such case the condition (ii) does not hold, although our DG method still improves the convergence rate than continuous FEM, the convergence rate is not optimal. Based on this consideration, we want to find other conditions for mesh grids, under which the proposed DG method could get optimal convergence rate.

4.2 Optimal Convergence Rate for 1D Case

For 1D case, we assume the condition (ii) does not hold. Since the solution of nonlocal problem (6) could be discontinuous across $\partial\Omega$, this discontinuity will be propagated to those points on $\partial\Omega_1$, which are δ distance from $\partial\Omega$. For such case, the best convergence rate to expect is $s = 1/2 - \epsilon$ for arbitrary small positive ϵ if continuous FEM is used. Theorem 6 improves the convergence rate from $1/2 - \epsilon$ to $3/2 - \epsilon$ for this case since we have the regularity of $H^{3/2-\epsilon}(\Omega)$. If the points on $\partial\Omega_1$ are selected as the mesh grids, the optimal convergence rate could be obtained.

Theorem 7 *Suppose $\gamma(x, y)$ satisfies (3), $b(x) \in C^1(\Omega) \cap H^2(\Omega_1) \cap H^2(\Omega_2)$, $\tilde{\gamma}(r) \in W^{1,1}(0, \delta)$. If δ and $1 - \delta$ are all selected as the mesh grids, then there exists a constant C such that, for sufficiently small h,*

$$\|u - u_h\|_{(0,1)} + h\|u' - u_h'\|_{(0,1)} \leq Ch^2\big(\|u\|_{2,(0,\delta)} + \|u\|_{2,(\delta,1-\delta)} + \|u\|_{2,(1-\delta,1)}\big). \quad (20)$$

Proof Using the interpolation error estimate in three intervals $(0, \delta)$, $(\delta, 1-\delta)$ and $(1-\delta, 1)$, respectively and add them together, we get

$$\|u - \mathcal{I}_h u\|_{(0,1)} \leq Ch^2\big(\|u\|_{2,(0,\delta)} + \|u\|_{2,(\delta,1-\delta)} + \|u\|_{2,(1-\delta,1)}\big).$$

Together with (16) and the inverse estimate we get (20). □

Remark 2 Due to the structure of the solution for the problem (6) we have discussed, the solution u is often discontinuous across $\partial\Omega$. For 1D case, it may cause the discontinuity of the first derivative across $\partial\Omega_1$ if $\tilde{\gamma}(r)$ has a discontinuity at $r = \delta$ (that is $\tilde{\gamma}(\delta) > 0$), or the discontinuity of the second derivative across $\partial\Omega_1$ if $\tilde{\gamma}(r)$ is continuous at $r = \delta$ (that is $\tilde{\gamma}(\delta) = 0$) but $\tilde{\gamma}'(r)$ has a discontinuity at $r = \delta$ (that is $\tilde{\gamma}'(\delta-) \neq 0$). In the next section, we will discuss two kinds of kernels representing the above two cases, respectively. While for 2D case, the solution of nonlocal problem often has higher regularity, the numerical experiments in Sect. 5 also confirm this point.

4.3 Condition Number Estimate

The condition number of the stiffness matrix is an indicator of the sensitivity of the discrete solution with respect to the data and the performance of iterative solvers such as the conjugate-gradient method. For the DG method we propose in Sect. 3, consider the $(m + n) \times (m + n)$

stiffness matrix A defined in (14). We have the following condition number estimate whose proof is standard and is given for completeness. Similar discussions can be found in earlier studies [1,38].

Theorem 8 *For the stiffness matrix A defined in (14) associated with the kernel $\gamma(\mathbf{x}, \mathbf{y})$ that satisfies (3), there exists a constant C such that*

$$\mathrm{cond}_2(A) \leq C.$$

Proof For the given finite element nodal basis, there exist two generic constants $c_2 \geq c_1 > 0$ such that

$$c_1 h^d |\mathbf{w}|^2 \leq \|w_h\|^2 \leq c_2 h^d |\mathbf{w}|^2, \quad \forall w_h = \sum_{j=1}^{m+n} w_j \widehat{\phi}_j \in V_{c,0}^{pc,h},$$

where $\{w_j\}$, $j = 1, 2, \ldots, m+n$, are components of the vector $\mathbf{w}$. Since the space $V_{c,0}(\Omega \cup \Omega_I)$ is equivalent to the space $L^2_{c,0}(\Omega \cup \Omega_I)$, we get the theorem immediately. □

We note again that the constant C may depend on the kernel, as demonstrated in [38], hence the result is only meaningful for nonlocal problems with a fixed kernel that satisfies the assumptions (3).

5 Numerical Results

We now report results of numerical experiments which substantiate the theoretical analysis in Sect. 4.

5.1 1D Numerical Experiments

For 1D case, the problem (6) becomes the following form

$$\begin{cases} -\int_{-\delta}^{\delta} \big(u(x+s) - u(x)\big)\gamma(s)ds = b(x) & \text{on } \Omega = (0,1), \\ u(x) = 0 & \text{on } \Omega_I = (-\delta, 0] \cup [1, 1+\delta). \end{cases} \tag{21}$$

We use the proposed DG method to solve the nonlocal problem first on uniform meshes and take δ to be a constant multiple of h and reduce h to check convergence and condition number properties, then on non-uniform meshes obtained by random disturbance to uniform ones. Here we choose two popular examples of kernel functions representing two cases as discussed in Remark 2 which is in $W^{1,1}(0, \delta)$, and one kernel function which is singular at the origin thus not in $W^{1,1}(0, \delta)$.

5.1.1 Constant Kernel Function

We first consider the following kernel function

$$\gamma(s) = \begin{cases} (2\delta)^{-1}, & |s| \leq \delta, \\ 0, & |s| > \delta. \end{cases} \tag{22}$$

Obviously γ defined as (22) is discontinuous at points $\pm\delta$, if b is discontinuous at points $x = 0$ or $x = 1$, the solution of (21) will probably be (however, not necessarily) discontinuous

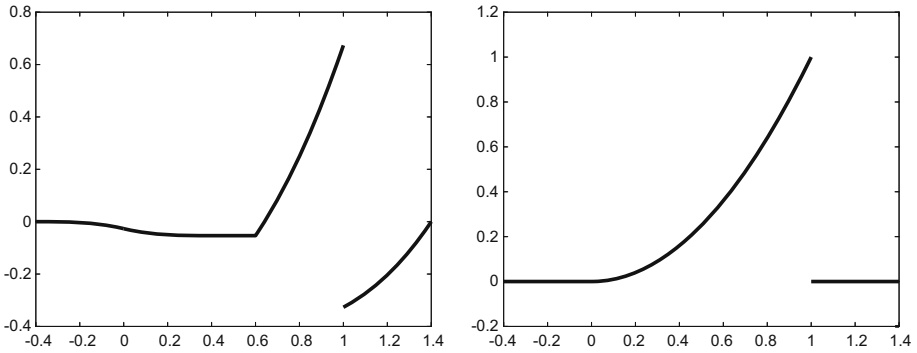

(a) $b(x)$ **(b)** $u(x)$

Fig. 1 Example 1: The right hand side function and the exact solution

Table 1 Example 1: Errors in L^2 and H^1 norms, corresponding convergence rates and spectral condition numbers on uniform meshes, *Cond* is abbreviation for the spectral condition number

δ/h	4	8	16	32	64
$\|u-u_h\|$	7.45e − 4	1.86e − 4	4.66e − 5	1.16e − 5	2.91e − 6
Rate	–	2.0000	2.0000	2.0000	2.0000
$\|u'-u_h'\|$	5.77e − 2	2.89e − 2	1.44e − 2	7.22e − 3	3.61e − 3
Rate	–	1.0000	1.0000	1.0000	1.0000
Cond	5.8875	6.7743	6.9926	7.0294	7.0282

in its first derivative at point $x = \delta$ or $x = 1-\delta$. In fact, in Example 1 the smoothness pick-up is beyond first order, that is, although b is discontinuous at point $x = 1$, u is infinitely continuously differentiable at point $x = 1-\delta$. While in Example 2 the smoothness pick-up is only first order and could not be improved, that is, since b is discontinuous at points $x = 0$ and $x = 1$, u' is is discontinuous at points $x = \delta$ and $x = 1-\delta$.

Example 1 In order to get simpler benchmark solutions, we calculate the right-hand side of (21) based on an exact solution $u(x) = x^2,\ x \in \Omega$ and $u(x) = 0,\ x \in \Omega_I$, with kernel function (22). This naturally leads to a δ-dependent right-hand side $b(x) = b_\delta(x)$, see Fig. 1 for the plots of $u(x)$ and $b(x)$. The DG method we proposed in Sect. 3 is used to numerically solve the problem (21) with $\delta = 0.4$.

We first use the proposed DG method on uniform meshes and conclude from Table 1 that convergence rates for errors in L^2 and H^1 norms are all optimal. The spectral condition number of the stiffness matrix is almost constant when the mesh size decreases, indicating the insensitivity of the discrete solution regardless how small h is.

We then use a kind of non-uniform meshes obtained by random disturbance to uniform meshes. To be specific, for a fixed m, let $h = \delta/m$, the non-uniform mesh is obtained by adding a random vector $\varepsilon \in \mathbb{R}^{m-1}$ (which obeys the uniform distribution on $[-0.1h, 0.1h]$) to x_i to reach $x_i + \varepsilon_i,\ i = 1, 2, \ldots, m-1$. Together with x_0 and x_m we get the new mesh grids

$$x_i^n = x_i + \varepsilon_i, \quad i = 1, 2, \ldots, m-1,\ x_0^n = x_0, \quad x_m^n = x_m. \tag{23}$$

Table 2 Example 1: Errors in L^2 and H^1 norms, corresponding convergence rates and spectral condition numbers on non-uniform meshes (23)

δ/h	4	8	16	32	64
$\|u - u_h\|$	8.04e − 4	2.50e − 4	6.00e − 5	1.24e − 5	3.14e − 6
Rate	–	1.6827	2.0629	2.2710	1.9846
$\|u' - u_h'\|$	5.84e − 2	2.95e − 2	1.48e − 2	7.30e − 3	3.65e − 3
Rate	–	0.9848	0.9965	1.0179	0.9983
Cond	5.9830	6.7507	7.0829	7.0786	7.0646

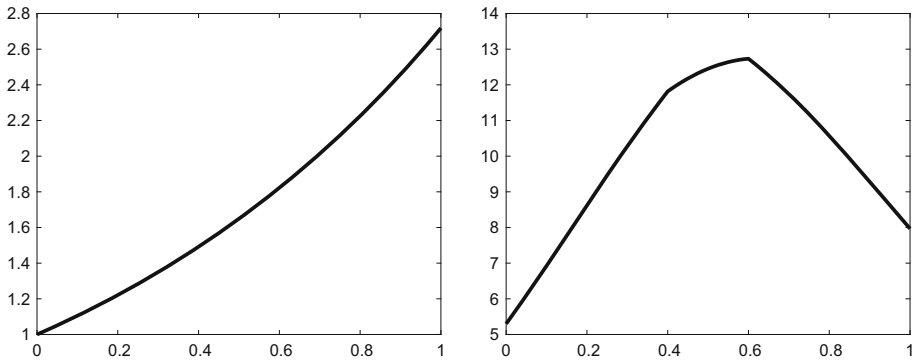

(a) $b(x)$ **(b)** $u_h(x)$

Fig. 2 Example 2: The right hand side function and the approximation solution

We have done over twenty tests, and the convergence rates and the spectral condition numbers are all similar. Thus, instead of listing all of them, we just select one test to verify our theoretical analysis. Similar actions and presentations are made also in later examples. It is seen from Table 2 that the errors in L^2 and H^1 norms and convergence rates are comparable with that in uniform meshes case. This is consistent with the theoretical result in Theorem 6 since $u \in C^\infty(\Omega)$, thus $s = 2$. The spectral condition numbers of the stiffness matrices behave similar as in the uniform meshes case, too.

Example 2 We consider (21) with kernel function (22) and $b(x) = e^x$. The proposed DG method is used to numerically solve the problem (21) with $\delta = 0.4$.

Since the exact solution $u(x)$ is not known for this problem we compute errors using the solution on finer meshes as approximation of the true solution. The proposed DG method is first used on uniform meshes. The right hand side function $b(x)$ and the approximation $u_h(x)$ with $h = 0.00625$ are plotted in Fig. 2. Although $b(x)$ is in $C^\infty(0, 1)$, it has two discontinuous points $x = 0$ and $x = 1$, which causes the discontinuity in the first derivative of u at points $x = \delta = 0.4$ and $x = 1 - \delta = 0.6$. From Table 3 it is seen that the method has optimal convergence rates for errors in L^2 and H^1 norms. The spectral condition numbers of the stiffness matrices for the method behave similarly as Example 1. Since the results for the spectral condition numbers of the stiffness matrices are all similar for the numerical tests in the rest of Subsect. 5.1, we no longer list them to avoid repetitions.

Next, we use the non-uniform meshes (23) to solve the problem. In this example the true solution $u(x) \in H^{1.5-\epsilon}(0, 1)$ for arbitrary small positive ϵ. So for general non-uniform

Table 3 Example 2: Errors in L^2 and H^1 norms, corresponding convergence rates and spectral condition numbers on uniform meshes

δ/h	4	8	16	32	64
$\|u-u_h\|$	7.54e − 3	1.79e − 3	4.38e − 4	1.08e − 4	2.69e − 5
Rate	–	2.0717	2.0349	2.0170	2.0084
$\|u'-u_h'\|$	4.90e − 1	2.41e − 1	1.19e − 1	5.94e − 2	2.97e − 2
Rate	–	1.0259	1.0114	1.0053	1.0026
Cond	5.8875	6.7743	6.9926	7.0294	7.0282

Table 4 Example 2: Errors in L^2 and H^1 norms, and convergence rates on non-uniform meshes (23)

δ/h	4	8	16	32	64
$\|u-u_h\|$	9.34e − 3	3.41e − 3	1.24e − 3	4.26e − 4	1.59e − 4
Rate	–	1.4519	1.4611	1.5411	1.4222
$\|u'-u_h'\|$	3.95e − 1	2.66e − 1	2.13e − 1	1.42e − 1	1.21e − 1
Rate	–	0.5712	0.3204	0.5815	0.3432

Table 5 Example 2: Errors in L^2 and H^1 norms, and convergence rates on non-uniform meshes (23) with δ and $1-\delta$ as grids

δ/h	4	8	16	32	64
$\|u-u_h\|$	6.98e − 3	1.72e − 3	4.10e − 4	1.01e − 4	2.49e − 5
Rate	–	2.0229	2.0661	2.0243	2.0180
$\|u'-u_h'\|$	4.17e − 1	2.14e − 1	1.01e − 1	4.74e − 2	2.42e − 2
Rate	–	0.9646	1.0781	1.0941	0.9671

meshes, we expect the convergence rates for errors in L^2 (H^1) norm to be at most 1.5 (0.5). This fact is verified in Table 4. However, as indicated in Theorem 7, since we know the two discontinuous points of $u'(x)$, if they are selected as mesh grids, optimal convergence rates could be recovered. To be specific, random disturbances are added to the original mesh grids except δ and $1-\delta$. The corresponding results are shown in Table 5. That is the convergence rates for errors in L^2 and H^1 norms are 2 and 1, respectively, which is consistent with the theoretical result (20). We then re-examine the computation on the meshes used in Table 4. The convergence rates, however, are not necessarily similar, which is different with Example 1. To be specific, if the perturbation for the points δ and $1-\delta$ is large in absolute value, such as $0.1h$, the convergence rates remain similar to Table 4. On the other hand, if the perturbation for the two points is small or close to zero, the convergence rates of the test are similar to Table 5. This phenomenon is very reasonable.

5.1.2 Linear Kernel Function

We then consider the kernel function

$$\gamma(s) = \begin{cases} (1-|s|/\delta)/\delta, & |s| \le \delta, \\ 0, & |s| > \delta. \end{cases} \tag{24}$$

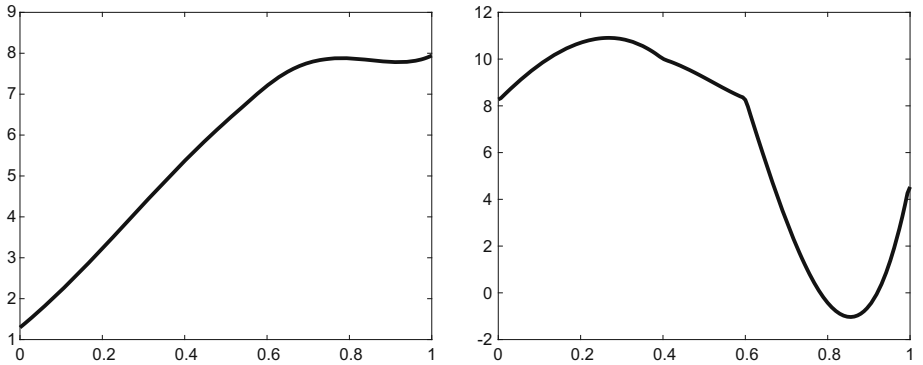

(a) $u_h(x)$ **(b)** $Z_h u_h'(x)$

Fig. 3 Example 3: The approximation solution and postprocessing of its derivative

Table 6 Example 3: Errors in L^2 and H^1 norms, and convergence rates on uniform meshes

δ/h	4	8	16	32	64
$\|u-u_h\|$	1.18e − 2	2.74e − 3	6.61e − 4	1.62e − 4	4.03e − 5
Rate	–	2.1019	2.0525	2.0246	2.0116
$\|u'-u_h'\|$	7.20e − 1	3.60e − 1	1.79e − 1	8.90e − 2	4.44e − 2
Rate	–	1.0018	1.0089	1.0056	1.0030

Obviously the $\gamma'(s)$ is discontinuous at points $\pm\delta$, if b is discontinuous at points $x = 0$ or $x = 1$, thus u'' will likely be discontinuous at points $x = \delta$ or $x = 1-\delta$. This is the case in Example 3 where the regularity pick-up is only second order and could not be further improved. That is, since b is discontinuous at points $x = 0$ and $x = 1$, u'' is discontinuous at points $x = \delta$ and $x = 1-\delta$.

Example 3 We consider (21) with kernel function (24) and $b(x) = 0.01e^{6x}$. The proposed DG method is used to numerically solve the problem (21) with $\delta = 0.4$.

As in Example 2, errors are computed using the solution on finer meshes as approximation of the true solution. We first implement the proposed DG method on uniform meshes. The approximation $u_h(x)$ with $h = 0.00625$ are plotted in Fig. 3. To see the discontinuity of the second derivative, a postprocessing of $u_h'(x)$, that is $Z_h u_h'(x)$ obtained by using the gradient recovery technique proposed by Zienkiewicz and Zhu [40] is also plotted in Fig. 3. Although $b(x) \in C^\infty(0,1)$, however, $b(x)$ has two discontinuous points $x = 0$ and $x = 1$, which causes the discontinuity for u'' at points $x = \delta = 0.4$ and $x = 1-\delta = 0.6$. From Table 6 it is seen that optimal convergence rates for errors in L^2 and H^1 norms are achieved.

Next, we use non-uniform meshes (23) to solve the problem. In this example the true solution satisfies $u(x) \in H^{2.5-\epsilon}(0,1)$ for arbitrary small positive ϵ. So for general non-uniform meshes the theoretical convergence rates for errors in L^2 and H^1 norms are all optimal. This is indeed verified in Table 7.

Table 7 Example 3: Errors in L^2 and H^1 norms, and convergence rates on nonuniform meshes (23)

δ/h	4	8	16	32	64
$\|u-u_h\|$	1.11e − 2	2.61e − 3	6.08e − 4	1.51e − 4	3.76e − 5
Rate	–	2.0891	2.0993	2.0143	1.9985
$\|u'-u_h'\|$	6.70e − 1	3.32e − 1	1.51e − 1	7.47e − 2	3.67e − 2
Rate	–	1.0128	1.1331	1.0189	1.0261

5.1.3 Singular Kernel Function

For $\alpha \in (0, 1)$ we consider the kernel function

$$\gamma(s) = \begin{cases} (1-\alpha)\delta^{\alpha-1}|s|^{-\alpha}/2, & |s| \le \delta, \\ 0, & |s| > \delta, \end{cases} \tag{25}$$

which satisfies (3), however, is singular at the origin and $\gamma(s) \notin W^{1,1}(0, \delta)$.

Example 4 We consider (21) with kernel function (25) and $b(x) = e^x$. The proposed DG method is used to numerically solve the problem (21) with $\delta = 0.4$.

Since the kernel function (25) satisfies (3), the solution $u(x)$ of (21) is continuous in $(0, 1)$. As in Example 2, errors are computed using the solution on finer meshes as approximation of the true solution, and then convergence rate is computed. We have implemented the proposed DG method on uniform meshes and non-uniform meshes (23) with δ and $1-\delta$ as grids, the convergence rates are similar, so we just list the results for uniform case.

Since the kernel function (25) is singular at the origin, $u(x) \in H^s(0, 1)$ with $s < 3/2-\alpha$. Here we want to analyze the regularity more carefully. The regularity of $u(x)$ in this example is determined by two factors: one is similar to Example 2, that is due to the discontinuity of $u(x)$ at point $x = 0$ and $x = 1$, $u'(x)$ is discontinuous across $x = \delta = 0.4$ and $x = 1-\delta = 0.6$; another one is the regularity of function $C_1 + C_2 x^{1-\alpha}$ $(x > 0)$ near point $x = 0$ and $C_3 + C_4(1-x)^{1-\alpha}$ $(x < 1)$ near point $x = 1$. With a uniform mesh or a generic non-uniform mesh (23) with δ and $1-\delta$ as grids, we can eliminate the regularity loss caused by the first factor, but not the second. In fact, using the idea of Theorem 7, we could prove for this example, the following error estimate holds

$$\begin{aligned} &\|u-u_h\|_{(0,1)} + h\|u'-u_h'\|_{(0,1)} \\ &\le Ch^{3/2-\alpha}\|u\|_{2,(0,\delta)} + Ch^{5/2-\alpha}\|u\|_{2,(\delta,1-\delta)} + Ch^{3/2-\alpha}\|u\|_{2,(1-\delta,1)} \\ &\le Ch^{3/2-\alpha}\big(\|u\|_{2,(0,\delta)} + \|u\|_{2,(\delta,1-\delta)} + \|u\|_{2,(1-\delta,1)}\big). \end{aligned} \tag{26}$$

The convergence rate after five steps is shown in Table 8 which confirms the theoretical result in part. As we see, convergence rate for $\alpha < 0.5$ is about $3/2-\alpha$ which is consistent with (26), however, for $\alpha > 0.5$ the convergence rate appears higher than $3/2-\alpha$. Nevertheless, if we continue to refine meshes, the convergence rate will approach to $3/2-\alpha$. To see this more clearly, we present the error history in the L^2 norm for $\alpha = 0.3$ and $\alpha = 0.9$, it is seen from the Fig. 4 that the convergence rate for $\alpha = 0.9$ is higher than $3/2-\alpha$ at earlier steps and then reduces to about $3/2-\alpha$ with the decrease of mesh size. This is due to the replacement for $\|u_h - u\|$ by $\|u_h - u_{2h}\|$. For larger α, the difference between these two estimates will be more evident for large mesh size. Thus, to get a more accurate reading on the convergence rate, we need to examine very small mesh sizes.

Table 8 Example 4: Convergence rates in L^2 norm for different α

α	0.1	0.2	0.3	0.4	0.5	0.6	0.7	0.8	0.9
Rate	1.410	1.295	1.194	1.100	1.010	0.926	0.851	0.788	0.739

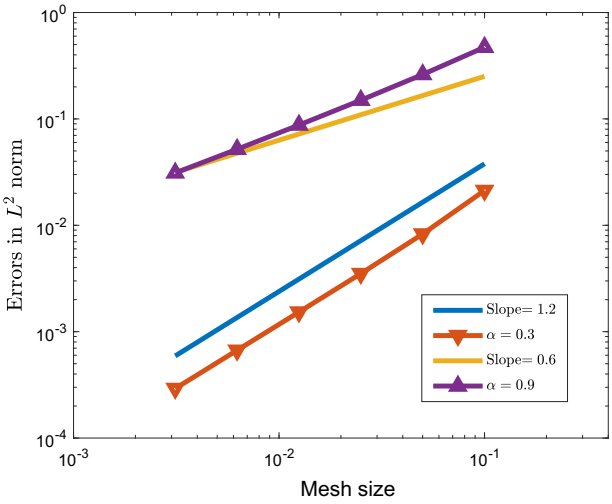

Fig. 4 Example 4: Errors in L^2 norm

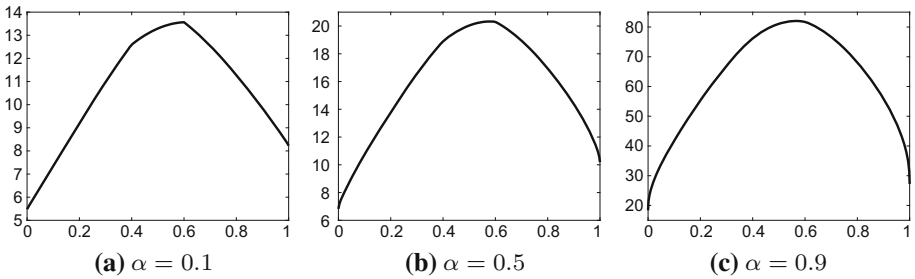

Fig. 5 Example 4: The approximation solution $u_h(x)$ for $\alpha = 0.1$, 0.5 and 0.9

We also plot the approximation solution for $\alpha = 0.1$, $\alpha = 0.5$ and $\alpha = 0.9$ in Fig. 5, which shows that the solution $u(x)$ of (21) with kernel function (25) behaves like function $C_1 + C_2(1-x)^{1-\alpha}$ $(x < 1)$ near point $x = 1$. This implies that the regularity of $u(x)$ could not exceed $H^{3/2-\alpha}(0, 1)$. In this case, we note that the use of graded meshes can help improving the convergence rate. The details are left for future studies.

5.2 2D Numerical Experiments

Here we discuss constant and linear kernel functions in the 2D case.

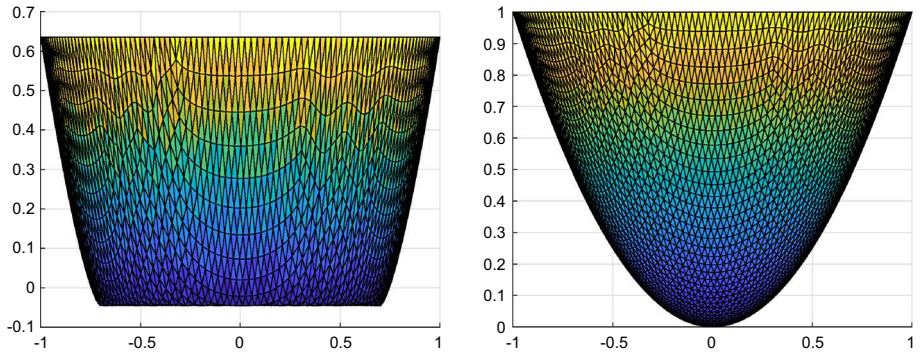

(a) $b(x)$ **(b)** $u(x)$

Fig. 6 Example 4: The right hand side function and the exact solution in x–z view

5.2.1 Constant Kernel Function

We first consider the following kernel function

$$\tilde{\gamma}(r) = \begin{cases} (\pi\delta^2)^{-1}, & r \le \delta, \\ 0, & r > \delta. \end{cases} \tag{27}$$

Example 5 In order to get simpler benchmark solutions, we calculate the right-hand side of (6) based on an exact solution $u(\mathbf{x}) = x_1^2 + x_2^2$, $\mathbf{x} = (x_1, x_2)^T \in \Omega = B_1(\mathbf{0})$ and $u(\mathbf{x}) = 0$, $\mathbf{x} \in \Omega_I = B_{1+\delta}(\mathbf{0}) \setminus \overline{B_1(\mathbf{0})}$, with kernel function (27). This naturally leads to a δ-dependent right-hand side $b(\mathbf{x}) = b_\delta(\mathbf{x})$, see Fig. 6 for the plots of $u(\mathbf{x})$ and $b(\mathbf{x})$. The proposed DG method is used to numerically solve the problem (6) with $\delta = 0.3$.

Although we could guarantee the quasi-uniformity of the triangulation, it is more suitable to plot errors versus number of vertices to show the convergence rate. From Fig. 7 it is seen that convergence rates for errors in L^2 and H^1 norms are optimal. Since the true solution is smooth enough, this result is not surprise. The spectral condition number of the stiffness matrix is almost constant when the mesh size is small enough, indicating the insensitivity of the discrete solution. Since the results for the spectral condition numbers of the stiffness matrices are all similar for the numerical tests in the rest of Subsect. 5.2, we no longer list them to avoid repetitions.

Example 6 We consider (6) with kernel function (27) and $b(\mathbf{x}) = 2x_1x_2$, $\mathbf{x} \in \Omega = B_1(\mathbf{0})$ and $u(\mathbf{x}) = 0$, $\mathbf{x} \in \Omega_I = B_{1+\delta}(\mathbf{0}) \setminus \overline{B_1(\mathbf{0})}$. The proposed DG method is used to numerically solve the problem (6) with $\delta = 0.3$.

Since the exact solution $u(\mathbf{x})$ is not known for this problem we compute errors using the solution on finer meshes as approximation of the true solution. From Fig. 8 it is seen that convergence rates for errors in L^2 and H^1 norms are all optimal, which confirms the result of Theorems 4 and 6 for 2D case.

5.2.2 Linear Kernel Function

We then consider the kernel function

$$\tilde{\gamma}(s) = \begin{cases} 3(1 - |s|/\delta)/\pi/\delta^2, & |s| \le \delta, \\ 0, & |s| > \delta. \end{cases} \tag{28}$$

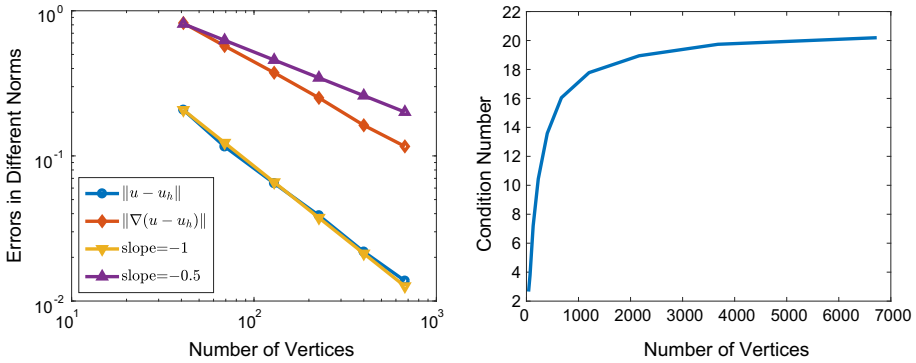

(a) Errors in different norms **(b)** Condition number

Fig. 7 Example 5: Errors in different norms and condition number

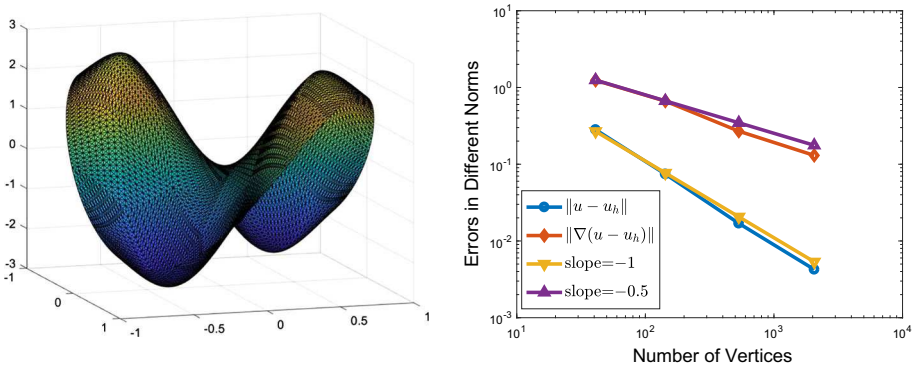

(a) $u_h(\mathbf{x})$ **(b)** Errors in different norms

Fig. 8 Example 6: The approximation solution and errors in different norms

Example 7 We consider (6) with kernel function (28) and $b(\mathbf{x}) = 2x_1x_2$, $\mathbf{x} \in \Omega = (0,1) \times (0,1)$ and $u(\mathbf{x}) = 0$, $\mathbf{x} \in \Omega_I = (-\delta, 1+\delta) \times (-\delta, 1+\delta) \setminus \Omega$. The proposed DG method is used to numerically solve the problem (6) with $\delta = 0.4$. From Fig. 9 it is seen that convergence rates for errors in L^2 and H^1 norms are all optimal.

6 Conclusion

We propose a new kind of DG method in this paper to numerically solve the nonlocal models with integrable kernels. The existed references tell us that if the right hand side function and the volume constraint function are in $L^2(\Omega)$ and $L^2(\Omega_I)$, respectively, the true solution of that nonlocal model also belongs to $L^2(\Omega \cup \Omega_I)$. Such a general result makes the numerical approximation difficult to operate, or easy to operate but not so efficiently. To make the approximation easier and more efficient simultaneously, we first convert the original nonhomogeneous problem with right hand side function in $L^2(\Omega)$ (if kernel function is integrable

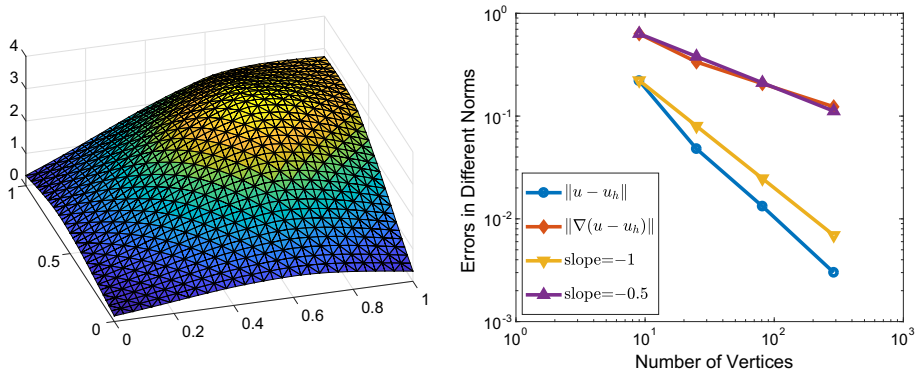

(a) $u_h(\mathbf{x})$ **(b)** Errors in different norms

Fig. 9 Example 7: The approximation solution and errors in different norms

however not square integrable, right hand side function and $g(\mathbf{x})$ should be in $L^\infty(\Omega)$ and $L^\infty(\Omega_I)$, respectively) to a homogeneous problem with right hand side function continuous in Ω. Then we analyze the structure of true solution of the homogeneous problem, especially for higher dimensional cases. The main result is, this kind of problem often encounters the discontinuity across the boundary $\partial\Omega$, thus possibly causes the discontinuity of first or second derivative (perhaps higher order derivatives, depending on the smoothness of the kernels and the dimensionality) across $\partial\Omega_1$. Based on this observation, an appropriate DG method is proposed which has some good properties, such as, the matrix of the algebraic system is symmetrical positive definite and has almost constant spectral condition number independent of the mesh size, the method is asymptotically compatible and uses less degrees of freedom compared with direct use of DG method. Moreover, it has optimal convergence rate for any dimensional case under mild assumptions. This is the essential improvement over the existed theory for standard approximation like continuous FEM.

References

1. Aksoylu, B., Unlu, Z.: Conditioning analysis of nonlocal integral operators in fractional Sobolev spaces. SIAM J. Numer. Anal. **52**, 653–677 (2014)
2. Aksoylu, B., Mengesha, T.: Results on nonlocal boundary value problems. Numer. Funct. Anal. Optim. **31**(12), 1301–1317 (2010)
3. Aksoylu, B., Parks, M.L.: Variational theory and domain decomposition for nonlocal problems. Appl. Math. Comput. **217**(14), 6498–6515 (2011)
4. Andreu-Vaillo, F., Mazón, J.M., Rossi, J.D., Julián T.-M.J.: Nonlocal diffusion problems. Number 165. American Mathematical Soc. (2010)
5. Arnold, D.N., Brezzi, F., Cockburn, B., Donatella Marini, L.: Unified analysis of discontinuous Galerkin methods for elliptic problems. SIAM J. Numer. Anal. **39**(5), 1749–1779 (2002)
6. Askari, E., Bobaru, F., Lehoucq, RB., Parks, ML., Silling, SA., Weckner, O: Peridynamics for multiscale materials modeling. In: Journal of Physics: Conference Series, vol. 125, p. 012078. IOP Publishing (2008)
7. Bobaru, F., Yang, M., Alves, L.F., Silling, S.A., Askari, E., Xu, J.: Convergence, adaptive refinement, and scaling in 1D peridynamics. Int. J. Numer. Methods Eng. **77**(6), 852–877 (2009)
8. Brenner, S., Scott, R.: The Mathematical Theory of Finite Element Methods, vol. 15. Springer, Berlin (2007)
9. Burch, N., Lehoucq, R.: Classical, nonlocal, and fractional diffusion equations on bounded domains. Int. J. Multiscale Comput. Eng. **9**(6), 661–674 (2011)

10. Chen, X., Gunzburger, M.: Continuous and discontinuous finite element methods for a peridynamics model of mechanics. Comput. Methods Appl. Mech. Eng. **200**(9), 1237–1250 (2011)
11. Chen, Z., Zou, J.: Finite element methods and their convergence for elliptic and parabolic interface problems. Numer. Math. **79**(2), 175–202 (1998)
12. Du, Q., Ju, L., Lu, J.: A discontinuous Galerkin method for one-dimensional time-dependent nonlocal diffusion problems. Math. Comput. **88**, 123–147 (2019)
13. Du, Q., Yang, J., Zhou, Z.: Analysis of a nonlocal-in-time parabolic equation. Discrete Contin. Dyn. Syst. B **22**(2), 339–368 (2017)
14. Du, Q.: An invitation to nonlocal modeling, analysis and computation. Proc. Int. Congr. Math. **3**, 3523–3552 (2018)
15. Du, Q.: Nonlocal modeling, analysis and computation. SIAM (2019)
16. Du, Q., Gunzburger, M., Lehoucq, R.B., Zhou, K.: Analysis and approximation of nonlocal diffusion problems with volume constraints. SIAM Rev. **54**(4), 667–696 (2012)
17. Du, Q., Gunzburger, M., Lehoucq, R.B., Zhou, K.: A nonlocal vector calculus, nonlocal volume-constrained problems, and nonlocal balance laws. Math. Models Methods Appl. Sci. **23**(03), 493–540 (2013)
18. Du, Q., Ju, L., Tian, L., Zhou, K.: A posteriori error analysis of finite element method for linear nonlocal diffusion and peridynamic models. Math. Comput. **82**(284), 1889–1922 (2013)
19. Du, Q., Tao, Y., Tian, X.: A peridynamic model of fracture mechanics with bond-breaking. J. Elast. **132**(2), 197–218 (2018)
20. Du, Q., Zhou, K.: Mathematical analysis for the peridynamic nonlocal continuum theory. ESAIM Math. Model. Numer. Anal. **45**(2), 217–234 (2011)
21. Emmrich, E., Weckner, O., et al.: On the well-posedness of the linear peridynamic model and its convergence towards the navier equation of linear elasticity. Commun. Math. Sci. **5**(4), 851–864 (2007)
22. Kilic, B., Madenci, E.: Coupling of peridynamic theory and the finite element method. J. Mech. Mater. Struct. **5**(5), 707–733 (2010)
23. Macek, R.W., Silling, S.A.: Peridynamics via finite element analysis. Finite Elem. Anal. Des. **43**(15), 1169–1178 (2007)
24. Oterkus, E., Madenci, E.: Peridynamic analysis of fiber-reinforced composite materials. J. Mech. Mater. Struct. **7**(1), 45–84 (2012)
25. Seleson, P., Parks, M.L., Gunzburger, M., Lehoucq, R.B.: Peridynamics as an upscaling of molecular dynamics. Multiscale Model. Simul. **8**(1), 204–227 (2009)
26. Silling, S.A.: Reformulation of elasticity theory for discontinuities and long-range forces. J. Mech. Phys. Solids **48**(1), 175–209 (2000)
27. Silling, S.A., Askari, E.: A meshfree method based on the peridynamic model of solid mechanics. Comput. Struct. **83**(17–18), 1526–1535 (2005)
28. Silling, S.A., Lehoucq, R.B.: Peridynamic theory of solid mechanics. Adv. Appl. Mech. **44**, 73–168 (2010)
29. Silling, S.A., Weckner, O., Askari, E., Bobaru, F.: Crack nucleation in a peridynamic solid. Int. J. Fract. **162**(1–2), 219–227 (2010)
30. Silling, S.A., Zimmermann, M., Abeyaratne, R.: Deformation of a peridynamic bar. J. Elast. **73**(1–3), 173–190 (2003)
31. Tao, Y., Tian, X., Du, Q.: Nonlocal diffusion and peridynamic models with Neumann type constraints and their numerical approximations. Appl. Math. Comput. **305**, 282–298 (2017)
32. Tao, Y., Tian, X., Qiang, D.: Nonlocal diffusion and peridynamic models with Neumann type constraints and their numerical approximations. Appl. Math. Comput. **305**, 282–298 (2017)
33. Tian, X., Qiand, D.: Analysis and comparison of different approximations to nonlocal diffusion and linear peridynamic equations. SIAM J. Numer. Anal. **51**(6), 3458–3482 (2013)
34. Tian, X., Qiang, D.: Asymptotically compatible schemes and applications to robust discretization of nonlocal models. SIAM J. Numer. Anal. **52**(4), 1641–1665 (2014)
35. Wang, H., Tian, H.: A fast Galerkin method with efficient matrix assembly and storage for a peridynamic model. J. Comput. Phys. **231**(23), 7730–7738 (2012)
36. Xu, F.: A multiscale implementation of finite element methods for nonlocal models of mechanics and diffusion. Ph.D. thesis, The Florida State University (2015)
37. Xu, F., Gunzburger, M., Burkardt, J.: A multiscale method for nonlocal mechanics and diffusion and for the approximation of discontinuous functions. Comput. Methods Appl. Mech. Eng. **307**, 117–143 (2016)
38. Zhou, K., Du, Q.: Mathematical and numerical analysis of linear peridynamic models with nonlocal boundary conditions. SIAM J. Numer. Anal. **48**(5), 1759–1780 (2010)
39. Zhou, K., Qiang, D.: Mathematical and numerical analysis of linear peridynamic models with nonlocal boundary conditions. SIAM J. Numer. Anal. **48**(5), 1759–1780 (2010)

40. Zienkiewicz, O.C., Zhu, J.Z.: A simple error estimator and adaptive procedure for practical engineerng analysis. Int. J. Numer. Methods Eng. **24**(2), 337–357 (1987)